NANO LETTERS

XXXX
Vol. xx, No. x
-

Mechanism and Optimization of pH Sensing Using SnO_2 Nanobelt Field Effect Transistors

Yi Cheng and P. Xiong*

Department of Physics and Center for Materials Research and Technology, Florida State University, Tallahassee, Florida 32306

C. Steven Yun and G. F. Strouse

Department of Chemistry and Biochemistry, Florida State University, Tallahassee, Florida 32306

J. P. Zheng

Department of Electrical and Computer Engineering, College of Engineering, Florida A&M University and Florida State University, Tallahassee, Florida 32310

R. S. Yang and Z. L. Wang

School of Materials Science and Engineering, Georgia Institute of Technology, Atlanta, Georgia 30332

Received June 13, 2008; Revised Manuscript Received September 22, 2008

ABSTRACT

We report a systematic investigation about the mechanism of pH sensing using SnO_2 nanobelt field effect transistors (FETs). The FETs, based on single SnO_2 nanobelts, are channel-limited and with proper contact passivation; the pH sensing was conducted with sodium phosphate solutions through integrated microfluidics. The responses of the FET channel conductance to pH were measured at different gate voltages: a linear pH dependence was observed in the linear transport "on" state, while an exponential dependence was observed in the subthreshold regime. Measurements at the same pH but different ion concentrations demonstrated that the FET's pH sensitivity decreases logarithmically with the ion concentration. The effect of APTES-functionalization was evaluated by comparing the pH responses of the same device with and without the surface modification. The APTES functionalization results in a slight enhancement of the pH sensitivity and a large suppression of the noise level, leading to marked improvement in the signal-to-noise ratio. The results indicate that the pH sensing is based on a screened field-effect response of the FETs to the surface protonation/deprotonation on the nanobelt. This study provides several useful guidelines for optimizing the sensor performance for chemical and biomolecular detection.

There is significant biomedical interest in developing rapid, portable, high-sensitivity pH sensors for very small amount of fluids. For example, the pH values of blood and interstitial are considered important indicators of human health.[1,2] The acid−base balance (or the concentration of H^+) in the extracellular fluid is tightly regulated and maintained by human buffer systems, lungs and kidneys (known as the homeostasis process), such that the pH of the arterial blood is maintained within a very tight range between 7.37 and 7.42.[3] This delicate balance is threatened continuously by additions of extra acids or bases to body fluids from either respiratory or metabolic processes. Exhaled breath, when condensed, forms the so-called exhaled breath condensate (EBC). This is another bodily fluid which can be analyzed for noninvasive identification of a variety of lung diseases and other biological markers.[4−6] Exhaled breath from deep within the lung is particularly useful in this regard; its molecular concentrations often correlate closely with those in the blood. Solid-state devices have shown great promise in achieving unprecedented speed, sensitivity, and portability in chemical and biomolecular sensing.[7] Modified semiconductor field-effect transistors (FETs) such as ion-sensitive FETs (ISFET)[8] and extended-gate FETs (EGFET)[9,10] have been extensively explored as pH sensors. The devices directly

* To whom correspondence should be addressed. E-mail: xiong@martech.fsu.edu.

10.1021/nl801696b CCC: $40.75
Published on Web 10/29/2008

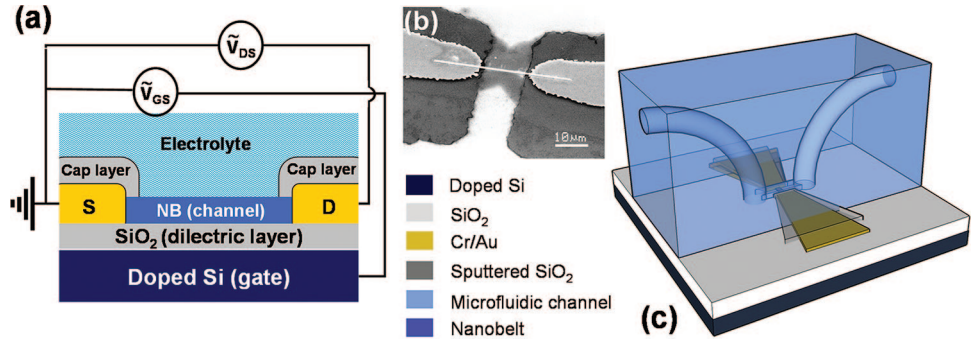

Figure 1. Schematic views of a SnO_2 nanobelt FET for solution pH sensing. (a) Side view of a SnO_2 nanobelt pH sensor and circuit diagram for field-effect measurements. (b) SEM image of a device with a SnO_2 nanobelt connecting the source/drain electrodes covered with sputtered SiO_2. (c) 3D schematic view of a SnO_2 nanobelt FET integrated with a PDMS microfluidic channel.

detect molecular bindings/reactions on the exposed gate dielectric surface, as the bindings/reactions cause local interfacial potential changes over the gate dielectric which alter the channel conductance. These schemes involve a separate reference gate electrode (either on-chip or stand-alone) which must make electrical contact with the analyte.[11]

More recently, there has been growing interest in utilizing FETs based on quasi one-dimensional (Q1D) semiconducting nanocomponents such as nanowires, nanotubes, and nanobelts for chemical and biological sensing.[12−15] The large surface-to-volume ratio of the nanomaterials optimizes the detection sensitivity. More importantly, since the critical dimensions of the Q1D nanocomponents are comparable or close to the sizes of many biological molecules, single-molecule detection of biosubstances such as virus, protein and DNA may be possible. The nanocomponents are routinely mass produced with vapor- or solution-phase techniques, and the FETs are most conveniently fabricated with a back-gate architecture which has two key advantages for solution chemical/biological sensing. First, the gate electrode is embedded in the device and not electrically connected to the solution (Figure 1a), which makes it possible to independently bias the FET to obtain optimum sensitivity. Second, the absence of a reference electrode which must be electrically connected to the solution could facilitate applications involving minute amount of fluids such as EBC.

Semiconducting oxide nanobelts, as one type of single-crystalline, uniform and stable Q1D nanostructures, are very attractive for chemical and biosensing applications. Among these binary oxide candidates, SnO_2 has long been a technologically important sensor material[16,17] and has been extensively studied in different forms (powder,[18] thin film,[19,20] and hybrid [21,22]) for gas sensing applications. However, to the best of our knowledge, there has been no report on their Q1D nanoscale counterpart for ion and biomolecular detection in aqueous solutions. Here we report the results of a series of pH sensing experiments with back-gated SnO_2 nanobelt FETs. Our devices employ the conventional MOSFET (metal-oxide-semiconductor field-effect transistor) structure. With a back gate and passivated source/drain electrodes, only the nanobelt channel is exposed to the solution.

The catalyst-free synthesis of the oxide nanobelts[23] and the fabrication and characterization of the FET devices have been described in detail previously.[24] In brief, high-performance SnO_2 nanobelt FETs were obtained on individual nanobelts on Si/SiO_2 substrates (degenerately doped n-Si with 100 nm thermal oxide). Cr/Au metallization produced low-resistance Ohmic source-drain contacts, which resulted in *channel-limited* FETs.[24] Such devices have been shown to be effective room-temperature hydrogen gas sensors.[24,25] For the application of in-solution sensing, the metal electrodes were passivated with 80 nm of SiO_2 deposited by magnetron sputtering as shown in Figure 1b. A microfluidic channel was made from SYLGARD 184 (DOW CORNING) poly dimethylsiloxane (PDMS) with a base/curing agent weight ratio of 7:1. After carefully removing air bubbles, the mixture was poured onto a Si mold prepared via photolithography and wet etching and baked at 65 °C in air for 20 h. The pattern had two reservoirs connected by a channel (100 μm wide and 80 μm high) and each with a 0.1 mm diameter inlet or outlet. The solidified transparent PDMS mold was placed on the nanobelt FET with the microfluidic channel covering the exposed portion of the SnO_2 nanobelt and parts of the passivated source/drain electrodes (Figure 1c). The solution flow was initiated via suction by a syringe pump on the outlet rather than pumping on the inlet, which facilitated rapid and smooth switching of different solutions in the flow without any pause in data collection. The flow rate was about 30 μL/min.

Prior to using a device for pH sensing, it was always characterized by standard two-probe I−V measurements to ensure that the device has Ohmic contacts and is channel-limited. All pH measurements were performed in the linear I−V region of the devices: a constant DC voltage of 0.1 V was applied between the source and drain electrodes using a Keithley 2400 source meter and the current was monitored at a resolution of 10 pA. Another identical source meter was used to apply the gate voltage for the field-effect measurements. The device and measurement setup were carefully grounded and shielded to minimize noise. All of the measurements were carried out at room temperature. Solutions with different pH values were prepared with a mixture of monobasic (NaH_2PO_4) and dibasic (Na_2HPO_4) sodium phosphates dissolved in DI water (resistivity > 18.5 MΩ cm). Phosphate ions are used as the buffer because they have three protonated forms (H_3PO_4, $H_2PO_4^-$, and HPO_4^{2-}) that have

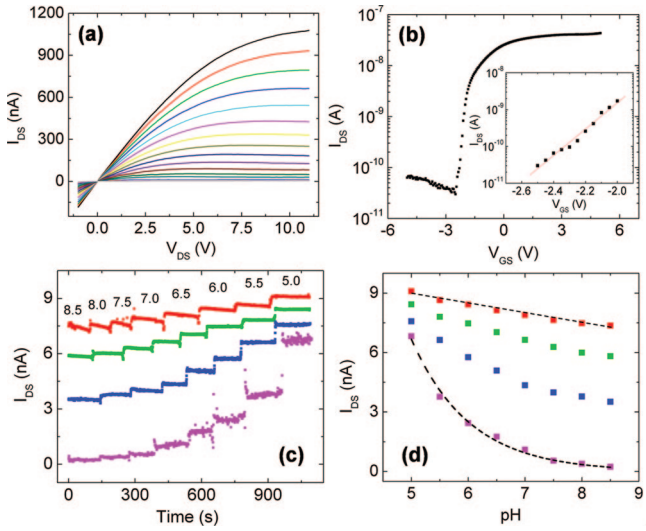

Figure 2. Characteristics and pH sensing of a SnO_2 nanobelt FET. (a) I_{DS} versus V_{DS} at V_{GS} from 5 to −5 V (top to bottom) in steps of 0.5 V, exhibiting typical n-channel depletion mode behavior. (b) Transfer characteristics, I_{DS} versus V_{GS} at $V_{DS} = 0.2$ V. Inset, the subthreshold regime showing a subthreshold swing of 280 mV/dec (c) Real-time I_{DS} responses to eight 10 mM sodium phosphate solutions of different pH at $V_{GS} = 2.0$, 0, −1.5, −2.5 V (from top to bottom). (d) I_{DS} versus pH at different gate voltage $V_{GS} = 2.0$, 0, −1.5, −2.5 V (from top to bottom). The dashed line and curve are linear and exponential fits to the data in the linear transport ($V_{GS} = 2.0$ V) and subthreshold ($V_{GS} = -2.5$ V) regimes respectively.

acid dissociation constant pK_a in the appropriate ranges (2, 7, and 12, respectively). The pH values of the solutions were determined by a pH meter with a resolution of 0.02 before their use in the sensing experiments.

Figure 2a and b shows the source-drain I−V and transfer characteristics of a typical SnO_2 nanobelt FET which is an n-channel depletion mode device. Figure 2a shows the $I_{DS} - V_{DS}$ at various gate modulations from 5 to −5 V in steps of 0.5 V. The I−V exhibit well-defined linear and saturation regimes and all pH sensing experiments were performed well within the linear regime. Figure 2b shows the transfer curve at $V_{DS} = 0.2$ V for the device with a subthreshold regime around $V_{GS} = -2.5$ V, which is shown more clearly in the inset: I_{DS} grows exponentially with V_{GS} which corresponds to a subthreshold swing of about 280 mV/decade. Figure 2c shows the real-time responses of the source-drain current of the SnO_2 nanobelt FET to 10 mM sodium phosphate solutions of different pH (from 5.0 to 8.5) at $V_{DS} = 0.1$ V and $V_{GS} = 2$, 0, −1.5, −2.5 V (top to bottom). There is a drift in I_{DS} for the curve at $V_{GS} = 2.0$ V, especially at high pH. This happens very rarely and we do not presently understand its origin. I_{DS} at a particular pH is then determined as the average of all data points taken at that pH. As shown in Figure 4d, I_{DS} decreases linearly with the pH of the solution at $V_{GS} = +2$ V, but there is a growing nonlinearity as V_{GS} decreases. I_{DS} approaches an exponential dependence on pH at $V_{GS} = -2.5$ V. The transition is shown quantitatively in Figure 2d: the pH response data in the subthreshold regime are well fit to an exponential function, $I_{DS} = C \exp(-\alpha \cdot pH)$, with $C = 900$ and $\alpha = 1.0$; for comparison, a

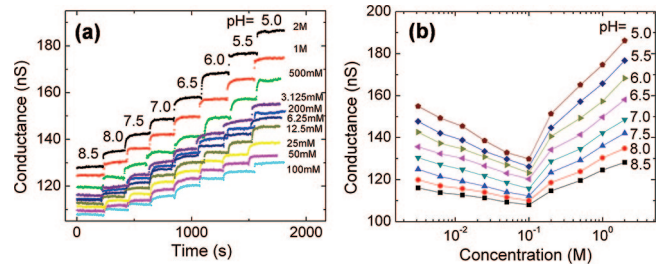

Figure 3. Channel conductance of a SnO_2 nanobelt FET in response to sodium phosphate solutions of pH values of 5.0, 5.5, 6.0, 6.5, 7.0, 7.5, 8.0, 8.5 and ten different molar concentrations (2000, 1000, 500, 200, 100, 50, 25, 12.5, 6.25, 3.125 mM): (a) real-time pH response of the device to 2000, 1000, 500, 3.125, 200, 6.25, 12.5, 25, 50, 100 mM sodium phosphate solutions (from top to bottom); (b) Channel conductance as a function of ten different ionic concentrations at different pH.

linear relationship is evident for the data at $V_{GS} = 2.0$V. The linear pH dependence of the FET channel conductance has been widely observed in devices based on a variety of semiconductor nanowires,[26−30] however, strongly nonlinear[12] and even exponential[13] dependences have also been seen. Our experiments demonstrate clearly that the pH dependence and sensitivity of a same nanowire FET can be varied by changing the transport regime. It is well-known that in a MOSFET the dependence of the source current on the surface potential is exponential in the subthreshold regime and linear in the linear transport regime. For FETs whose channel surface has highly reactive functional sites (e.g., −OH) and when the electrolyte concentration is relatively low, a linear dependence of the surface potential on the electrolyte pH is expected from previous calculations[11] and a more recent modeling,[31] which consequently produces a linear pH dependence within the linear transport regime ("on" state, above threshold) and an exponential dependence in the subthreshold regime.

Concurrent with the increasing nonlinearity as V_{GS} decreases, the pH sensitivity is significantly enhanced. However, there is a pronounced increase in the noise level inside the subthreshold regime. There are two major sources for the higher noise in the subthreshold regime. The first is a consequence of the low carrier density in the subthreshold regime, which, according to Hooge's law,[32,33] results in a more significant impact by the carrier number fluctuations on the noise spectra. The other is the exponential dependence of the channel conductance in the subthreshold regime, in which any ion adsorption/desorption on the nanobelt surface or charge trapping/detrapping in the dielectric is expected to result in larger fluctuations in the channel conductance. Similar observations have been reported and discussed on FET devices based on other Q1D nanocomponents.[34,35] Therefore, the gate modulation as well as the materials parameters of the nanowire should be tuned to optimize the signal-to-noise ratio (SNR) for sensing applications.

In Figure 3 we present the results of pH sensing experiments aimed at evaluating the effects of the ion concentration of the solutions. Figures 3(a) shows the real-time responses the average channel conductance of a SnO_2 nanobelt FET in response to sodium phosphate solutions of different pH

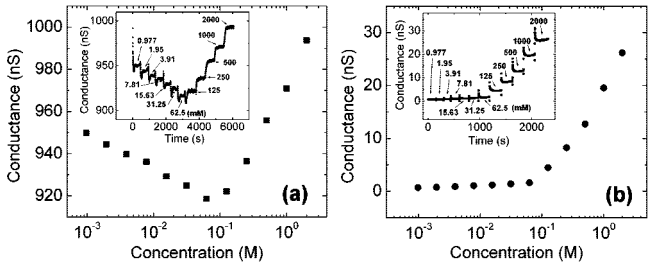

Figure 4. Effects of ion concentration: (a) SnO_2 nanobelt channel conductance as a function of ion concentration of NaCl electrolytes (pH = 7.0) at 0.977, 1.95, 3.91, 7.81, 15.63, 31.25, 62.5, 125, 500, 1000, 2000 mM. Inset: real-time response of the channel conductance as a function of electrolyte ion concentration. (b) Conductance of a similarly constructed device, with partially exposed electrodes and without a nanobelt, in the presence of NaCl solutions of different concentrations. Inset: real-time response of the device to the NaCl electrolytes. The solution concentrations and microfluid flow sequence are identical to those used in (a).

values from 5.0 to 8.5 at ten different molar concentrations (2000, 1000, 500, 200, 100, 50, 25, 12.5, 6.25, 3.125 mM). In Figure 3(b), the FET channel conductance is plotted as a function of the ionic concentrations for all pH values measured. It is evident that the pH sensitivity of the device is not monotonic with the ion concentration: the channel conductance at the same pH initially decreases logarithmically with increasing ion concentration and then turns around. The pH sensitivity, defined as $\Delta G/G_0$ per pH, follows a similar dependence on the ion concentration.

In order to quantify the observed ion concentration dependence and elucidate its origin, we performed detailed measurements of the channel conductance of a SnO_2 nanobelt FET in response to an extensive set of electrolyte samples of phosphate buffers, sodium chloride solutions and their mixtures, with a broad range of ion concentrations. All experiments yield qualitatively similar conductance dependences on the concentration. The results for a series of NaCl solutions whose ion concentration spans more than three decades are shown in Figure 4a. As the solution flow changes from low (0.977 mM) to high (2 M) concentration in steps of 2×, the channel conductance exhibits an initial decrease and then a fast increase from a concentration of about 70 mM. The initial conductance decrease with ion concentration has a clear logarithmic dependence spanning nearly 2 orders of magnitude of ion concentrations. The logarithmic dependence is consistent with the simulation of ref 31, which originates from electrostatic screening of the overall charge effectiveness of the hydrogen ions by the ions in the sodium chloride solution. The subsequent conductance increase from 70 mM to 2 M is most likely due to the increasing contribution of ionic conduction. Although the electrodes are insulated from the solution by sputtered SiO_2, the electrolyte forms a parallel conduction path through the nanobelt. In order to verify this conjecture and estimate the contribution from ionic conduction in the overall signal, we performed an identical set of measurements on a similarly constructed control device. The device was similar to the nanobelt FET but was without a nanobelt and several micrometers of the electrodes at the edges were left uncovered by the SiO_2. The conductance of the control device as a function of the NaCl solution concentration is shown in Figure 4b, and the real-time response to the solution flow is shown in the inset. The conductance across the device is negligibly small until the NaCl concentration reaches about 70 mM, which coincides with the turning point in the data shown in Figure 4a. Quantitatively, the measured conductance increases from approximately zero at 0.1 mM to ~30 nS at 2 M, which is in reasonable agreement with the apparent ionic conduction contribution to the channel conductance in Figure 4a, considering the structural differences of the two devices.

The data in Figure 3, from a set of sodium phosphate buffer solutions at pH from 5.0 to 8.5, are also consistent with the results of the control experiment. Especially, the increases in the measured conductance at high ion concentrations are in good quantitative agreement with the ionic conduction contribution identified in Figure 4. These results clearly demonstrate that there is significant contribution to the measured conductance from ionic conduction at high enough ion concentrations. However, it is also clear that in the low buffer concentration range of biomedical and technological significance for pH and biomolecular using nanowire FETs, ionic conduction is negligibly small. In this regime, the FET's pH sensitivity decreases with increasing buffer concentration. The results suggest that, in addition to modulating the channel conductance/carrier density of the nanobelt, the electrolyte concentration should be optimized to minimize the screening effect due to the salt ions.

In an effort to explore means of enhancing the sensitivity and stability of the device in pH sensing, we have examined the effects of chemical modification of the nanobelt surface with APTES (3-Aminopropyltriethoxysilane). For the assembly of APTES monolayer on the SnO_2 nanobelt, a freshly made device was cleaned with oxygen plasma for 8 min, and then soaked in 1% PEG-silane (2-methoxy-(polyethyleneoxy)propyl trimethoxysilane) for 6 h followed by 2% APTES for 20 h. The PEG-silane bind to and passivate the SiO_2 so that the APTES assemble selectively onto the SnO_2 nanobelt surface by means of a longer treatment time.[36] A schematic diagram and an SEM image of a device after APTES treatments are shown in Figure 5a and b, respectively. The determination of the above optimal procedure was based on a set of fluorescence experiments verifying successful passivation of the SiO_2 and selective binding of APTES to the SnO_2 nanobelt. For the fluorescence microscopy imaging, the sample was further treated with D-biotin (succinimidyl ester) in DMF (N,N-Dimethylformamide) buffer and fluorescently labeled (Alexa-488) streptavidin in MES (2-Morpholinoethanesulfonic acid, monohydrate) buffer and thoroughly rinsed with DI water. The result is shown in the fluorescence image in Figure 5c from which the highly selective functionalization of the SnO_2 nanobelt channel is clearly evidenced.

A direct comparison of the conductance responses to pH for the same SnO_2 nanobelt FET with and without surface APTES-functionalization is shown in Figures 6. Time dependent channel conductance of the device with APTES treatment in response to 50 mM sodium phosphate solutions

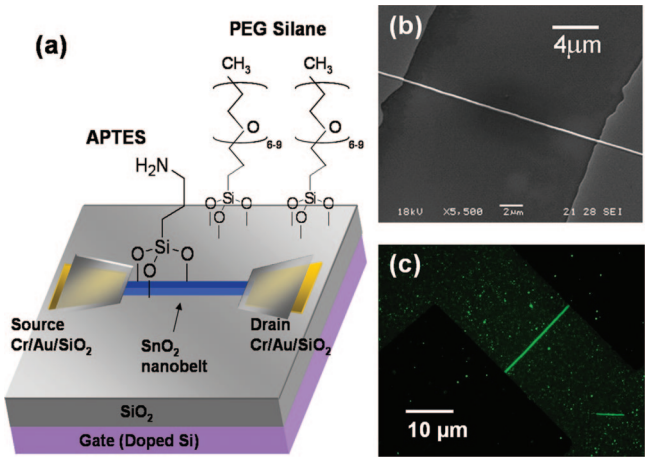

Figure 5. (a) Schematic view of a nanobelt FET device after PEG-silane passivation of SiO_2 and APTES functionalization of the SnO_2 channel. (b) SEM image of a SnO_2 nanobelt FET. (c) Fluorescence image of a SnO_2 nanobelt FET showing highly selective surface functionalization of the SnO_2 channel.

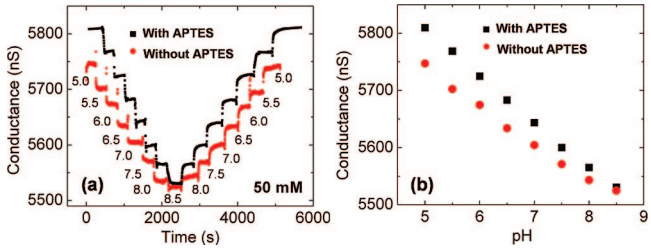

Figure 6. Effects of APTES functionalization: (a) Conductance of a SnO_2 nanobelt FET with (black) and without (red) surface APTES modification versus time in 50 mM sodium phosphate solutions of different pH. (b) Conductance versus pH value with (black) and without (red) surface APTES modification. The gate bias is zero in both cases.

of pH from 5.0 to 8.5 was first measured, and the results are shown in Figure 6a (black dots). The APTES on the nanobelt was then removed by piranha cleaning of the device. An identical set of measurements were repeated to obtain the device response without APTES functionalization (Figure 6a, red dots). The pH responses of the device with and without APTES functionalization are qualitatively similar, as shown in Figure 6b. For both cases, the conductance varies linearly with the pH of the solution with slopes of 81 nS/pH and 64 nS/pH in the presence and absence of APTES respectively. In an aqueous environment, it is known that there is high density of hydroxyl groups on an unfunctionalized oxide surface. Therefore, it is likely that the pH sensitivity there stems from reaction of the hydroxyl groups with the H^+ in the solution ($Sn - O^- + H^+ \leftrightarrow Sn - OH$ and $Sn - OH + H^+ \leftrightarrow Sn - OH_2^+$). On the other hand, the pH response of the APTES-functionalized devices is probably predominantly from the protonation/deprotonation of the amine end groups ($-NH_2 + H^+ \leftrightarrow -NH_3^+$ and $-O^- + H^+ \leftrightarrow -OH$), although some $-OH$ groups may still be present and contribute to the conductance change. As a result, the APTES functionalization leads to slightly higher pH sensitivity for the device. Moreover, the APTES functionalization suppresses the noise level, probably due primarily to the higher proton affinity of the surface amine groups. The passivation of the SiO_2 substrate by PEG silane may also contribute to the lower noise. The inert $-CH_3$ group of PEG silane prevents the nonspecific protonation/deprotonation on the SiO_2 surface; this effect on areas within the Debye screening length of the nanobelt channel could suppress charge fluctuations. Thus, it may be a combination of the APTES functionalization of the nanobelt and PEG-silane passivation of the gate dielectric surface that lead to a marked improvement (more than a factor of 3) in the signal-to-noise ratio.

As alluded to before, the linear pH dependence for APTES-functionalized and unmodified devices in the "on" state is somewhat surprising since in the classical diffusion-capture model one would expect the conductance change to be directly proportional to the H^+ concentration and therefore depends exponentially on the pH ($pH = -\log[H^+]$). A recent modeling of nanowires biosensors takes into account the electrostatic screening by ions in the electrolyte[31] and the intrinsic buffer capacity of the oxide surface.[37] In the "on" state of the FET, linear pH dependences for the channel conductance were deduced for $OH + NH_2$ surface functionalization in the entire pH range and for OH functionalization only when $pH > 5$.[31] Our observations on both bare (OH only) and APTES-functionalized ($OH + NH_2$) nanobelts are in good agreement with the predictions. In previous experiments of pH sensing with various types of nanowire FETs, the linear pH dependence was widely observed.[12,30] As demonstrated earlier, the occasional observations of exponential[13] pH dependence was most likely due to the device operating in the subthreshold regime of the FETs.

It is worthwhile, at this point, to compare the pH sensitivity of the different devices studied in this work. We compare three unfunctionalized nanobelt FETs shown in Figures 2, 3, and 6, at zero gate bias. Although the ion concentrations are somewhat different (10 mM, 12.5 mM, and 50 mM for the first, second, and third device respectively), a qualitative trend is clear from the comparison: the pH sensitivity is the highest for the device with the smallest intrinsic conductance (Figure 2, 12.8% per pH) and the lowest for the device with the largest intrinsic conductance (Figure 6, 1.16% per pH). However, the noise level is significantly lower for the device with high channel conductance, resulting in similar SNR for the two cases; thus a better SNR is expected for the high conductance device at the same ion concentration. This is understandable since a similar density of surface protonation/deprotonation should induce a larger relative change in the channel conductance for a device with a nanobelt of smaller thickness and/or carrier density, while the noise level is expected to be lower for a nanobelt with high conductivity. The results are in good agreement with the trends revealed through back gate tuning of the FET as shown in Figure 2(c). Taken together, these results suggest a number of ways to optimize the SNR of pH and biomolecular sensing using nanowire FETs.

In summary, the mechanism of pH sensing by SnO_2 nanobelt FETs and various factors affecting its sensitivity have been systematically investigated. The results are

consistent with a pH sensing mechanism based on a screened field-effect response of the FETs to the surface protonation/deprotonation on the nanobelt. Back gate modulation is capable of significantly alter the pH response of a device, with a linear pH dependence for the channel conductance in the "on" state and exponential dependence in the subthreshold regime. The electrostatic screening by salt ions leads to a logarithmic decrease of pH sensitivity with the ion concentration in low concentration range absent of ionic conduction. APTES functionalization of the SnO_2 nanobelt results in slight enhancement of the pH sensitivity and large suppression of the noise level, leading to marked improvement in the device's SNR. The experimental results offered a number of useful guidelines for optimizing the sensing performance and demonstrated the efficacy of the oxide nanobelt FETs as stable pH and biomolecular sensors.

Acknowledgment. We thank Drs. Jing Yuan and Linda Hirst for assistance with the fluorescence imaging and Drs. Linda Hirst, David Van Winkle, Stephan von Molnár, and Pradeep Nair for valuable discussions. This work was supported by NSF NIRT Grant No. ECS-0210332, NIH NIGMS grant GM079592, and a FSU Research Foundation PEG grant.

References

(1) Arieff, A. I.; DeFronzo, R. A. *Fluid, Electrolyte and Acid-Base Disorders*; Churchill Livingstone: New York, 1995.
(2) Gamble, J. L. *Acid-Base Physiology: A Direct Approach*; The Johns Hopkins University Press: Baltimore, MD, 1982.
(3) Barron, K. W. *Physiology (Oklahoma Notes)*, 4th ed.; Springer: New York, 1995.
(4) Mutlu, G. M.; Garey, K. W.; Robbins, R. A.; Danziger, L. H.; Rubenstein, I. *Am. J. Respir. Crit. Care Med.* **2001**, *164*, 731–737.
(5) Kharitonov, S. A.; Barnes, P. J. *Am. J. Respir. Crit. Care Med.* **2001**, *164*, 731–737.
(6) Hunt, J. *J. Allergy Clin. Immunol.* **2002**, *110* (1), 28–34.
(7) Taylor, R. F.; Schultz, J. S. *Handbook of Chemical and Biological Sensors*, 1st ed.; Institute of Physics Publishing: Philadelphia, PA, 1996.
(8) Liao, H.-K.; Wu, C.-L.; Chou, J.-C.; Chung, W.-Y.; Sun, T.-P.; Hsiung, S.-K. *Sens. Actuators, B* **1999**, *61* (1−3), 1–5.
(9) Batista, P. D.; Mulato, M. *Appl. Phys. Lett.* **2005**, *87*, 143508.
(10) Chi, L. L.; Chou, J. C.; Chung, W. Y.; Sun, T. P.; Hsiung, S. K. *Mater. Chem. Phys.* **2000**, *63*, 19–23.
(11) Madou, M. J.; Morrison, S. R. *Chemical Sensing with Solid State Devices*; Academic: Boston, MA, 1989.
(12) Cui, Y.; Wei, Q.; Park, H.; Lieber, C. M. *Science* **2001**, *293*, 1289.
(13) Stern, E.; Klemic, J. F.; Routenberg, D. A.; Wyrembak, P. N.; Turner-Evans, D. B.; Hamilton, A. D.; LaVan, D. A.; Fahmy, T. M.; Reed, M. A. *Nature* **2007**, *445*, 519–522.
(14) Wang, W. U.; Chen, C.; Lin, K.-h.; Fang, Y.; Lieber, C. M. *Proc. Natl. Acad. Sci. U.S.A.* **2005**, *102*, 3208.
(15) Arnold, M.; Avouris, P.; Pan, Z. W.; Wang, Z. L. *J. Phys. Chem. B* **2003**, *107*, 659.
(16) Liu, Y.; Koep, E.; Liu, M. *Chem. Mater.* **2005**, *17* (15), 3997–4000.
(17) Yang, J.-W.; Cho, H.-J.; Lee, S.-H.; Lee, J.-Y. *Environ. Monit. Assess.* **2004**, *92* (1−3), 153–161.
(18) Behr, G.; Fliegel, W. *Sens. Actuators, B* **1995**, *26/27*, 33.
(19) Hoefer, U.; Bottner, H.; Felske, A.; Kuhner, G.; Steiner, K.; Sulz, G. *Sens. Actuators, B* **1997**, *44* (1), 429–433.
(20) Yea, B.; Konishi, R.; Osaki, T.; Abe, S.; Tanioka, H.; Sugahara, K *Appl. Surf. Sci.* **1996**, *100/101*, 365.
(21) Matsubara, I.; Hosono, K.; Murayama, N.; Shin, W.; Izu, N. *Mater. Res. Soc. Symp. Proc.* **2004**, *785*, D14.9.
(22) Pourfayaz, F.; Khodadadi, A.; Mortazavi, Y.; Mohajerzadeh, S. S. *Sens. Actuators, B* **2005**, *108* (1−2), 172–176.
(23) Pan, Z. W.; Dai, Z. R.; Wang, Z. L. *Science* **2001**, *291*, 1947.
(24) Cheng, Y.; Fields, L. L.; Yang, R. S.; Zheng, J. P.; Wang, Z. L.; Xiong, P. *Appl. Phys. Lett.* **2006**, *89*, 093114.
(25) Fields, L. L.; Cheng, Y.; Xiong, P.; Zheng, J. P. *Appl. Phys. Lett.* **2006**, *88*, 263102.
(26) He, J. H.; Zhang, Y. Y.; Liu, J.; Moore, D.; Bao, G.; Wang, Z. L. *J. Phys. Chem. C* **2007**, *111* (33), 12152–12156.
(27) Al-Hilli, S. M.; Al-Mofarji, R. T.; Willander, M. *Appl. Phys. Lett.* **2006**, *89* (17), 173119–173121.
(28) Park, I.; Li, Z.; Li, X.; Pisano, A. P.; Williams, R. S. *Biosens. Bioelectron.* **2007**, *22* (9−10), 2065–2070.
(29) Chen, Y.; Wang, X.; Erramilli, S.; Mohanty, P.; Kalinowski, A. *Appl. Phys. Lett.* **2006**, *89*, 223512–223514.
(30) Kang, B. S.; Ren, F.; Heo, Y. W.; Tien, L. C.; Norton, D. P.; Perton, S. J. *Appl. Phys. Lett.* **2005**, *86*, 112105.
(31) Nair, P. R.; Alam, M. A. *Nano Lett.* **2008**, *8* (5), 1281–1285.
(32) Weissman, M. B. *Rev. Mod. Phys.* **1988**, *60*, 537–571.
(33) Dutta, P.; Horn, P. M. *Rev. Mod. Phys.* **1981**, *53*, 497–516.
(34) Wang, W.; Xiong, H. D.; Edelstein, M. D.; Gundlach, D.; Suehle, J. S.; Richter, C. A. *J. Appl. Phys.* **2007**, *101*, 044313.
(35) Lin, Y.-M.; Appenzeller, J.; Knoch, J.; Chen, Z.; Avouris, P. *Nano Lett.* **2006**, *6*, 930.
(36) Moses, P. R.; Wier, L.; Murray, R. W. *Anal. Chem.* **1975**, *47* (12), 1882.
(37) Bergveld, P.; van Hal, R. E. G.; Eijkel, J. C. T. *Biosens. Bioelectron.* **1995**, *10*, 405–414.

NL801696B